THE JOURNAL OF PHYSICAL CHEMISTRY B

Article

pubs.acs.org/JPCB

Water Barrier Properties in Biaxially Drawn Poly(lactic acid) Films

Nicolas Delpouve,[†] Grégory Stoclet,*[,‡] Allisson Saiter,[†] Eric Dargent,*[,†] and Stéphane Marais[§]

[†]AMME-LECAP, EA 4528 International Laboratory, Institute of Material Research FED4114, Université de Rouen, Faculté des Sciences, Avenue de l'Université BP 12, 76801 Saint Etienne du Rouvray, France

[‡]Université de Lille Nord de France, UMR CNRS 8207, Unité Matériaux et Transformations, Université Lille1 Sciences et Technologies, Batiment C6, 59655 Villeneuve d'Ascq, France

[§]Université de Rouen, Laboratoire PBS UMR 6270 CNRS & FR 3038INC3M 76821 Mont-Saint-Aignan Cedex, France

ABSTRACT: Crystallization is among the easiest ways to improve polymer barrier properties because of the tortuosity increase within the material and the strong coupling between amorphous and crystalline phases. In this work, poly(lactic acid) (PLA) films have undergone α' thermal crystallization or different drawing processes. Although no effect of α' thermal crystallization on water permeability is observed, the drawing processes lead to an enhancement of the PLA barrier properties. This work clearly shows that, in the case of PLA, the crystallinity degree is not the main parameter governing the barrier properties contrary to the crystalline and amorphous phase organizations which play a key role. X-ray analyses confirm that the macromolecular chain orientation in the amorphous phase is the main cause of the improvement of the drawn PLA water barrier property. This improvement is due to the orthotropic structure formation for sufficient draw ratios, particularly when using the Simultaneous Biaxial drawing mode. Moreover, independently of the draw conditions, the drawing process tends to reduce the plasticization coefficient. Consequently, the drawn material barrier properties are not much affected by the water passage.

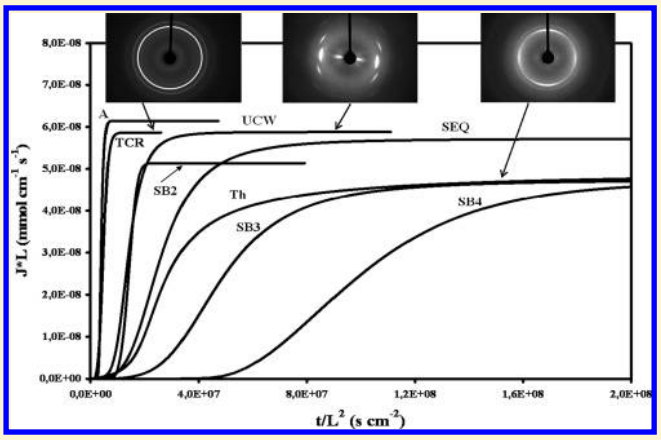

1. INTRODUCTION

In recent years, environmental concerns have increased the interest in elaborating biodegradable packaging materials to replace commonly used plastics issued from petrochemistry. Nevertheless using these kinds of polymers in such applications involves combining their ecofriendly character with a number of specific functional requirements such as sufficient mechanical, thermal or barrier properties. Many works have shown the possibilities offered by the use of biodegradable polymers in the packaging field. Poly(lactic acid) (PLA), a biodegradable polyester issue from renewable resources, shows a promising applicability due to its mechanical performances better than polystyrene (PS) ones,[1] and its similarities with PET.[2,3] Consequently, the interest in studying PLA barrier properties has risen and it has been shown that PLA exhibits medium gas barrier properties[4] and poor water barrier properties.[5] Most articles investigating PLA gas barrier properties have revealed that the CO_2 permeability coefficient of PLA is lower than the coefficient of PS and higher than the CO_2 permeability coefficient of PET.[6] Similar results have been observed regarding to the 0_2 permeation properties.[7,8]

In order to outclass this property lack, the composites and nanocomposites elaboration routes have been tested.[4,9−11] Filling PLA with nanoclays, cellulose fibers (for low fiber content),[12] microcrystalline cellulose,[13] or β-anhydrite[14] or by incorporating PLA into a blend[15] has shown an improvement of these properties. For example, Zenkiewicz et al.[11] reported a permeability decrease included between 10 and 27% in the case of PLA nanocomposites elaborated by extrusion blowing. Particularly these authors have shown that, in the case of PLA/MMT nanocomposites, this process induces a parallel ordering along sample's thickness of the Montmorillonite platelets, increasing the barrier properties particularly for a blow ratio of 4. Another route investigated was the elaboration of laminates with PLA. Indeed Cho et al.[16] have shown that the barrier properties can be increased by this method.

When studying the barrier properties of PLA, it is obvious that the microstructure has to be considered. Indeed, permeability and diffusivity in semicrystalline polymers are thought to decrease with increasing crystallinity.[17] However, in the case of PLA, it has been reported that gas transport properties could be independent of the crystallinity degree.[18] Indeed Colomines et al.[19,20] have obtained from oxygen and helium permeation measurements similar permeability coefficients between an amorphous PLA and a semicrystalline PLA elaborated by compression-molding. Authors deduced that the barrier properties are not influenced by the crystalline phase degree. However, Tsuji et al.[21] have presented opposite

Received: December 5, 2011
Revised: March 5, 2012
Published: March 20, 2012

conclusions: they observed an increase in the barrier properties when PLA crystallizes at 140 °C from 0 to 30%. Considering these results it appears that the PLA crystallization protocol, which leads to different microstructures, plays an important role on the barrier properties.

PLA is a broad class of polyesters usually containing both L and D stereoisomer units in various amounts. This involves a complex crystallization behavior with low crystallization kinetics. Moreover, different crystalline forms have been put in evidence depending on the thermomechanical history.[22−24]

The water barrier property dependence to the polymorphic structure, i.e., to the crystallization temperature, has been recently evidenced by Cocca et al.:[25] the α crystals formed at $T \geq 145$ °C provide better water barrier properties as compared to films containing less perfect α' crystals formed at $T \leq 95$ °C. Although the relationships between barrier properties and thermal isotropic crystallization have already been established,[26] it remained unclear how the drawing process could affect the barrier properties. Drawing a polymer promotes the formation of an oriented structure. For example it has been shown for PET that barrier properties can be improved in that way.[27,28] In initially amorphous PLA also, it has been shown that an oriented crystalline phase can be induced when the material is stretched above its glass transition temperature,[29−32] so an improvement of barrier properties is expected.

Characterization and understanding of anisotropy effects on the PLA water barrier properties are thus of prime interest in order to improve properties. As a consequence, this work is aimed at studying the effect of the drawing process used on microstructure and water properties of PLA. To reach this goal, three drawing modes have been tested: Uniaxial Constant Width (UCW) drawing, Simultaneous Biaxial (SB) drawing, and Sequential Biaxial (SEQ) drawing.

2. EXPERIMENTAL SECTION

2.1. Material. The polylactide (PLA) investigated in this work, containing 4.3 mol % of D-isomer units, was purchased from Natureworks (grade 4042D). The number-average and weight-average molecular weights are M_n = 116 kDa and M_w = 188 kDa, respectively, as measured by GPC. Pellets were compression-molded during 15 min in a SCAMEX 20 T into films between steel plates at 185 °C under a pressure of 100 bar, before being quenched to 273 K during a very short time in ice water in order to afford crystallization. The amorphous character of the PLA film has been controlled using DSC. The glass transition temperature and melting temperature, determined by means of DSC, are located around 327 and 428 K, respectively.

2.2. Drawing Processes. Drawing experiments are carried out on a Cellier tenter frame consisting of four pantographs each equipped with ten pneumatic grips. More details about the equipment are given in ref 33. The two movable pantographs are driven by hydraulic jacks. Square specimens of 100 × 100 mm^2 gauge widths were used. Samples were stretched at T_d = 70 °C, i.e., between the glass transition and crystallization temperatures, at a constant jack speed of 1 mm s^{-1}, i.e., an initial stretching speed of 0.01 s^{-1}. The true strains of the samples were determined from a square grid of 1 × 1 cm^2 mesh size printed on the sample prior to drawing.

Three drawing modes were used in this study. In UCW drawing mode, the films are drawn only in one direction called the machine direction (MD) or the longitudinal direction (LD) while the film is constrained in the perpendicular direction called the transverse direction (TD). In SB drawing mode, the films are simultaneously drawn in two perpendicular directions at the same rate and to the same ratio. During SEQ drawing, the films are first drawn in MD in UCW mode. Then, the films are drawn in TD in UCW mode. The same stretching rate is used in MD and TD. The draw ratio λ is defined as $\lambda = L/L_0$, where L_0 is the gauge length and L the macroscopic sample length assessed from the jack displacement.

The draw ratios λ achieved in this study are respectively 3 × 1 (UCW), 3 × 3 (SEQ), and 2 × 2, 3 × 3, and 4 × 4 (SB) where $\lambda = \lambda_{MD}\lambda_{TD}$. A last sample consisting in a sample drawn in SB drawing mode up to a draw ratio of 3 × 3 and thermofixed, i.e. annealed at 393K (T_g + 60 K) during ten minutes, has been also studied.

2.3. Permeation Measurements. Water permeation tests are performed using a permeation apparatus constituted of a measurement cell (a dry nitrogen supply) and a hygrometric unit as the sensor (chilled mirror hygrometer, Gruter & Marchand, France). The film under test is placed in the permeation cell (effective area A = 2.5 cm^2) and dry nitrogen is flushed into both compartments for many hours (at least 20 h) until a constant dew point temperature is obtained (around 210 K). After this dry step, a stream of liquid water is pumped through the upstream compartment. The water concentration in the initially dry sweeping gas is monitored in the downstream compartment via the hygrometer and a data acquisition system. The flux of water vapor $J(L, t)$ at t time at the dry interface is obtained from

$$J(L, t) = \frac{f}{A}10^{-6}\frac{(x^{out} - x^{in})}{RT}p_t \quad (1)$$

where L is the film thickness, t the time, f the flow of nitrogen, R the ideal gas constant and T the temperature of the experiment. The water concentration x (in ppmV) is calculated from the water vapor pressure p, which is directly related to the sweeping gas dew points T_{dp} at the inlet and the outlet of the cell ($x = 10^6 p/p_t$, p_t being the total pressure, usually 1 atm). All the water permeation tests are carried out at 25 °C on a surface of 2.5 cm^2 as the rest of the film is protected by a seal mask and is not accessible for water. This procedure allows controlling exactly the draw ratio of the film undergoing diffusion and obtaining a very homogeneous thickness (the variation on the thickness never exceeds 10 μm for amorphous and thermally crystallized samples and 4 μm for drawn samples). The thickness of each film is measured using a numerical caliper on different points. The reproducibility of the measure is checked on 4 amorphous samples (with respective thicknesses of 229, 204, 157, and 287 μm), 3 thermally crystallized samples (169, 175, and 225 μm), 2 UCW (60 and 88 μm), SB3 (22 and 30 μm), SEQ (38 and 38 μm), and thermofixed samples (30 and 32 μm). One measurement is carried for SB2 (94 μm) and SB4 (15 μm) samples.

The mathematical treatment of diffusion transport through the film sample is based on the following assumptions:[34,35] (i) the polymer film is dense and homogeneous, (ii) the process is Fickian, (iii) the interfacial sorption equilibrium is instantaneous, and (iv) the mass transfer occurs in a direction perpendicular to the plane sheet. Concentration and flux

profiles, $C(x,t)$ and $J(x,t)$, are described by Fick's laws and the boundary conditions used are

$$\begin{aligned} &\text{for} \quad t = 0, \quad C(x, 0) = 0 \quad \forall\, x \in]0, L[\\ &\text{at} \quad x = 0, \quad C(0, t) = C_{eq} \quad \forall\, t \\ &\text{at} \quad x = L, \quad C(L, t) = 0 \quad \forall\, t \end{aligned} \tag{2}$$

The theoretical flux curve exhibits a sigmoidal shape which can be divided into two steps: the transient step and then the stationary step. The permeability coefficient P is obtained from the steady state flux with

$$P = \frac{J_{st} L}{\Delta a} \tag{3}$$

where J_{st} is the stationary flux and Δa, practically equal to 1, is the difference in water activity between the two faces of the film. In order to examine the possible variation of diffusivity with water concentration, the diffusion coefficient D is calculated at two different times of the extent of permeation process

- The time t_I, corresponding to $J/J_{st} = 0.24$, i.e., to the inflection point of the transient permeation curve[36]

$$D_I = \frac{0.091 L^2}{t_I} \tag{4}$$

- The time-lag t_L, corresponding to $J/J_{st} = 0.62$[37]

$$D_L = \frac{L^2}{6 t_L} \tag{5}$$

When the values of D_L and D_I are practically equal, D can be assumed to be constant.

2.4. Temperature Modulated Differential Scanning Calorimetry (TMDSC). For each film tested in permeation, a piece nonexposed to water is taken for thermal analysis. TMDSC experiments are performed on a TA Instruments apparatus (DSC 2920) equipped with a low-temperature cell (minimal temperature = 203 K). Nitrogen is used as purge gas (70 mL/min). The samples weights are about 2 mg, encapsulated in standard DSC aluminum alloy pans, and disposed in a way to have the best thermal contact possible. Before the experiments, samples are stored in vacuum desiccators over P_2O_5 for at least two weeks to avoid moisture sorption effects. Calibration in temperature and energy is normally carried out, using standard values of melting temperature T_f and fusion enthalpy ΔH_f for indium (T_f = 429.75 K and ΔH_f = 28.66 J/g).[38] The TMDSC experiments are performed with oscillation amplitude of 0.318 °C, oscillation period of 60 s and heating rate of 2 K min^{-1}. Thus, the analysis is carried in the Heat-Only mode which is advised for the crystallization and fusion study in semicrystalline polymers.[39] The standard enthalpy used for the PLA crystallinity degree calculation was taken equal to 93 J/g.[40] The complete deconvolution procedure proposed by Reading et al. is used in these experiments, allowing the obtaining of the reversing and nonreversing Heat Flows.[41,42]

2.5. Wide Angle X-ray Scattering (WAXS). Wide-angle X-ray scattering (WAXS) analysis is carried out owing to a Panalytical sealed tube operating at 40 kV and 20 mA. The Cu Kα radiation (λ = 1.54 Å) is selected with a Nickel filter. The WAXS patterns are recorded on 2D CCD camera (Photonic Sciences). Through-view and edge-view 2D-patterns are collected for each sample. In order to determine the strain-induced structure, a qualitative analysis is performed starting from the 180°-azimuthally integrated profiles calculated using the FIT2D software. Drawn samples are analyzed along their faces and their edges in order to characterize the texturation of the material. When analyzed along their edges samples are placed vertically.

3. RESULTS

Figure 1a,b depict the mechanical behavior of PLA stretched at T_d = 70 °C until a draw ratio λ = 3 × 3 in simultaneous and

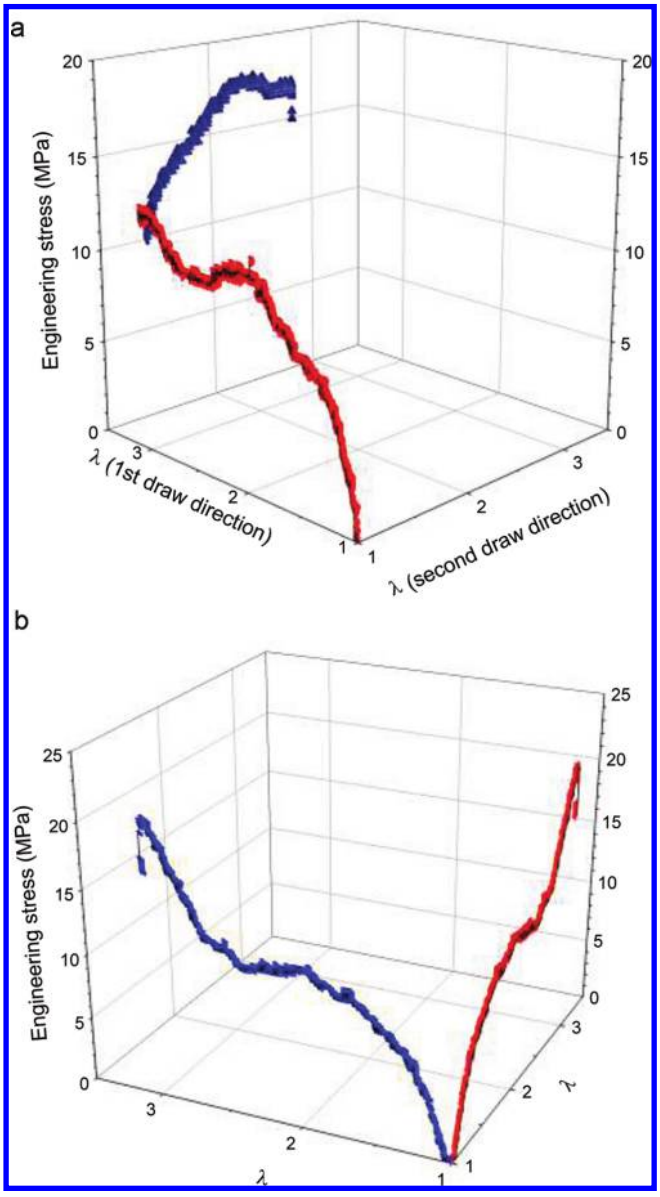

Figure 1. Mechanical behavior of PLA samples (a) sequentially drawn and (b) simultaneously drawn.

sequential modes respectively. Two stages can be observed independently with the drawing process. First, for small elongation ratios the material behaves like a rubbery material for the different stretching modes. Then, for λ > 2, a strain hardening phenomenon occurs until sample's break. This strain hardening phenomenon has ever been reported in the case of

dx.doi.org/10.1021/jp211670g | J. Phys. Chem. B 2012, 116, 4615–4625

PLA uniaxial stretching and has been ascribed to a strain-induced structuration of the material that is to say to the formation of a crystalline phase and/or a mesophase depending on the drawing conditions.[30−32] Finally one can note that sample's break occurs for draw ratios around 4 independently with the drawing mode.

WAXS patterns obtained for the drawn materials are depicted in Figure 2. For sake of clarity the flat-on patterns

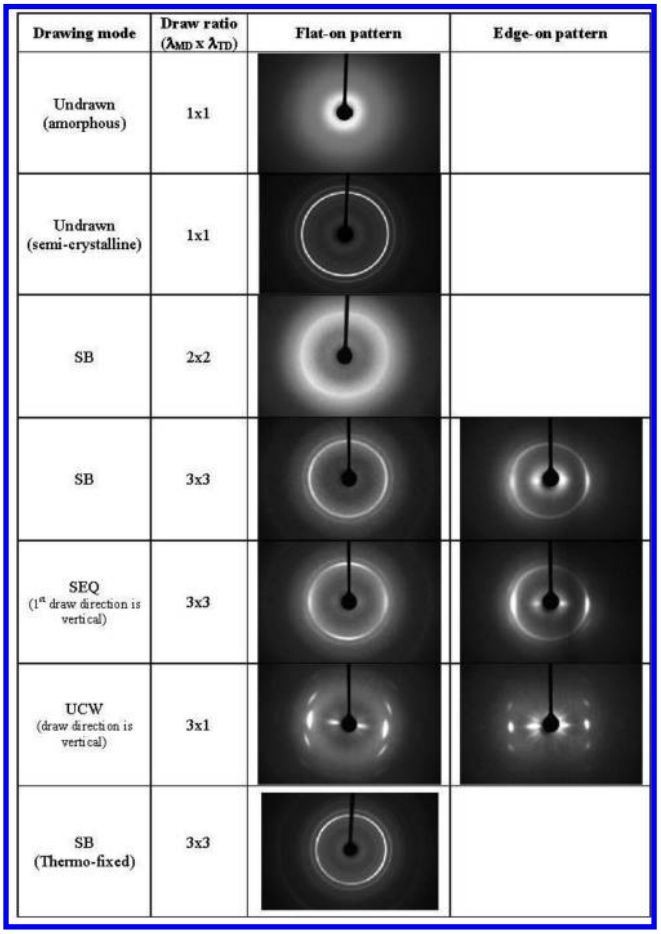

Figure 2. WAXS patterns of drawn and thermally crystallized PLA films obtained normally to the film plane (*XY*n) and through the film thickness (*XY*e).

will be denoted *XY*n while the edge-on patterns will be denoted *XY*e, *X* being the drawing mode used and *Y* the elongation ratio achieved. The WAXS pattern obtained for the initial material (i.e., $\lambda = 1 \times 1$) exhibits a diffuse amorphous halo characteristic of a fully isotropic amorphous material. Regarding the SB drawn material with a draw ratio of 2×2 (SB2n), that is to say at the beginning of the strain hardening stage, the WAXS pattern exhibits a weak diffraction ring having a low intensity indicating, first that a small amount of crystals has been induced upon stretching and second that the strain-induced crystalline structure is nearly isotropic. For a higher draw ratio (SB3n), the clear intensification of the main diffraction ring associated with the appearance of a second ring shows a substantial increase of the strain-induced crystallinity degree. Moreover, even if the draw ratio has increased, the strain-induced crystalline structure is still nearly isotropically distributed along the sample's thickness. In opposition the WAXS pattern obtained from flat-on view (SB3e) shows an anisotropic structure as revealed by the presence of the two intensity reinforcements around the equator. Since these two equatorial arcs are ascribed to the (200)/(110) diffraction planes, this indicates a preferential orientation of the crystals in the plane of the film.[43] As a consequence, these results obtained for the SB drawing mode show that a strain-induced crystallization phenomenon occurs above $\lambda = 2$, the crystallinity degree increasing with increasing strain, and that the strain-induced crystals have an orthotropic orientation. In other words crystals are rather laid down along sample's thickness and nearly isotropically distributed in the plane of the film.

Now regarding the SEQ drawn material, the flat-on WAXS pattern (SEQ3n) slightly differs from the one recorded at the same draw ratio in the SB mode. Indeed the latter shows the presence of a diffraction ring with four intensifications arcs located along both the equator and the meridian. This means that, contrary to the SB case, where the crystals were isotropically distributed, two preferential crystallization directions exist in the SEQ case, these directions corresponding to the two stretching directions. Regarding to the WAXS pattern along the thickness of the sample SEQ3e and SB3e, one can still observe a reinforcement of the intensity along the equator, meaning that crystals are rather laid down along sample's thickness. The behavior observed for SEQ mode can be explained from the strain induced structure in UCW mode as this mode corresponds to the first stage of SEQ mode. As revealed by the WAXS pattern recorded for the sample stretched at $\lambda = 3 \times 1$, which in fact shows the strain-induced structure induced during the first step of the SEQ mode, a strong uniaxial texturation of the material is observed. The two intense equatorial diffraction arcs indicate that crystals oriented along the draw direction have been induced upon stretching. Assuming that the same behavior occurs during the second drawing stage, this explains the four intensifications observed on the SEQ3n pattern. The same kind of pattern is obtained from the edge-on view (UCW3e), even if the diffraction spots are weaker, meaning a more pronounced orientation of the crystals along the plane of the film. In this way it is worth noticing that in the UCW case, the strain induced structure is not cylindrically symmetrical, contrary to the case of unconstrained uniaxial drawing.[30] Finally, regarding the effect of a postdrawing thermal treatment, the thermofixed material (Th) obtained from annealing the SB3 sample, exhibits an intense and weak diffraction ring indicating that the annealing process induces an isotropization of the strain induced crystals. The same behavior is observed in the case of the stabilization of SEQ3 sample (results not shown here).

To summarize, it has been shown that the strain-hardening phenomenon observed on the stress−strain curves is related to a strain-induced crystallization phenomenon. Moreover, the strain-induced structure is very sensitive to the drawing process used, and in all cases the drawing process induces a preferential orientation of strain-induced crystals. Indeed the crystals are distributed in a way that the denser planes are lying in the film plane. This is in agreement with previous results reported by Ou et al.[44,45] even if the PLA grade used here is not the same. Furthermore, the integrated intensity profiles have been computed from the WAXS patterns and reported in Figure 3a,b for the SB3n and SEQ3n samples respectively. Two peaks appear at $2\theta = 16.4°$ and $2\theta = 18.6°$. These two peaks are respectively ascribed to (200)/100 and (203) diffraction planes of the α' crystalline form (i.e., the disordered α form).[24]

dx.doi.org/10.1021/jp211670g | *J. Phys. Chem. B* 2012, 116, 4615−4625

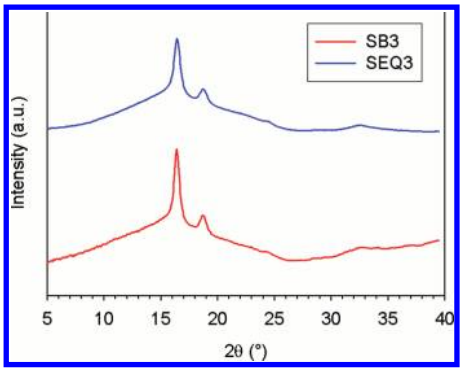

Figure 3. Integrated intensity profiles of SB3 (a) and SEQ3 (b).

Thus the crystalline phase induced upon biaxial stretching is the same than the one obtained in the case of uniaxial stretching in equivalent draw conditions. This is in good agreement with previous results, showing that this crystalline form is induced for samples thermally or mechanically crystallized at temperatures below 120 °C.[30,31]

Structural characterization of drawn PLA samples has been completed by TMDSC analyses, particularly with the aim of quantifying the different phase contents induced upon stretching. The average heat flow obtained for the different materials are presented in Figure 4. The quenched film exhibits first at 327 K a heat flow step characteristic of the glass transition, then a very large crystallization peak ranging from 370 to 420 K, and finally a complex fusion peak around 425 K. This kind of peak is generally attributed to polymorphic α and α' crystalline forms undergoing melt-recrystallization in the same temperature range.[46] A shift of T_g appears to higher temperatures for crystallized samples since the amorphous phase needs more energy to relax. Nevertheless, for all drawn samples, it is obvious that the glass transition does not appear sufficiently clearly to allow the heat flow step analysis. This is mainly caused by the presence of an exothermic peak in the same temperature range (333−353 K). This behavior has already been observed in PLA by Kulinsky et al.[47] who ascribe this exothermic peak to a cold-crystallization phenomenon. When cold crystallization and glass transition occur in almost the same temperature range, crystallization and melting phenomena are analyzed on the Average Heat Flow signal while the glass transition is analyzed for each material regarding to the Reversing Heat Flow signal presented in Figure 5.[48] Indeed TMDSC allows separating thermal events related to the glass transition from kinetic events. Several phenomena are visible on these curves: (i) The glass transition domain is larger for highly drawn or thermally crystallized materials as structural heterogeneities induce a widening of the relaxation time distribution.[49] (ii) An endothermic peak attributed to the mesophase transformation is observable in the glass transition of the SEQ material.[31] (iii) The presence of a sub-Tg exothermic peak for the SB2 material is caused by the release of the mechanically induced excess enthalpy.[50,51] (iv) Finally in most of the samples, the amplitude of the reversing heat flow step is lesser than in the amorphous one. As shown in Figure 6a the crystallinity degree X_c is obtained from the crystallization and fusion enthalpies in the average heat flow signal. From the prolongation of the liquid state and the glassy state lines in the Reversing Heat Flow signal (Figure 6b), the reversing heat flow step is obtained. This value is proportional to the heat capacity step and the quantity of amorphous phase relaxing at the glass transition, i.e., the mobile amorphous phase content X_{am} is deduced. Calculated results are reported in Table 1 (with the uncertainties corresponding to the standard deviations). Considering the different SB drawn samples, the crystallinity degree increases from 13% to 31% when the draw ratio increases from 2 × 2 to 4 × 4. The highest crystallinity achieved at $\lambda = 4 \times 4$ is equivalent to the one obtained in the case of uniaxial drawing in the same conditions, and seems to be the maximum crystallinity achievable by this grade of PLA. Also, this crystallinity maximum corresponds to the one reported for the same PLA grade stretched in unconstrained uniaxial drawing.[30] In drawn samples $X_c + X_{am}$ is almost equal to 1, i.e., no drawn sample exhibits higher X_{ar} value than 10%. The calculus of X_{ar} is made from X_c and X_{am} values and the resulting standard deviation is higher than 5%. Consequently, the 2-phases

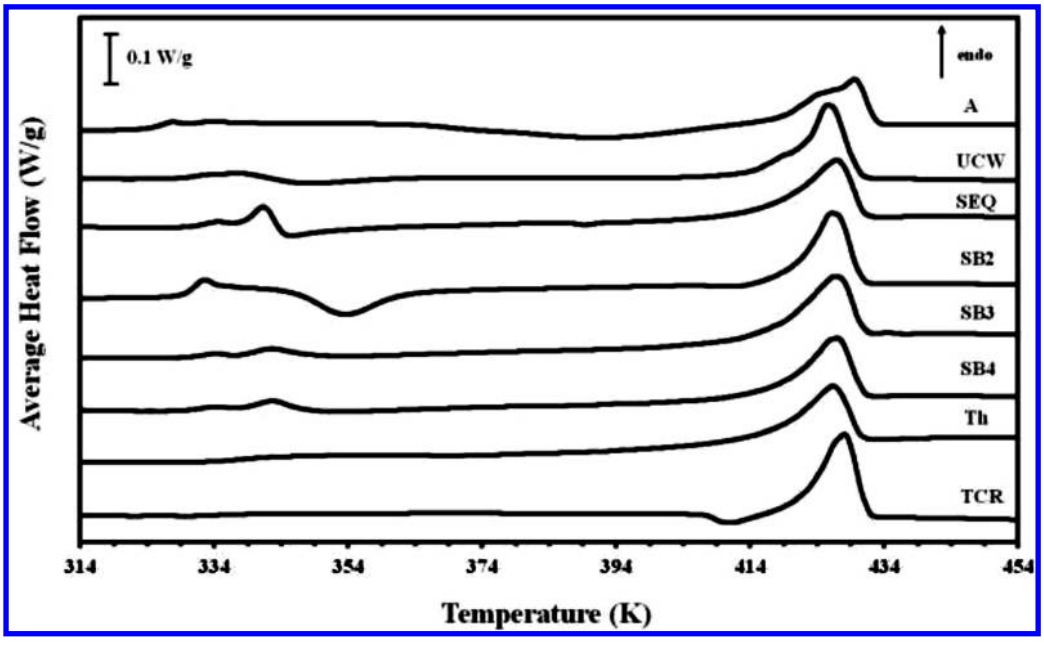

Figure 4. Average heat flow versus temperature.

dx.doi.org/10.1021/jp211670g | J. Phys. Chem. B 2012, 116, 4615−4625

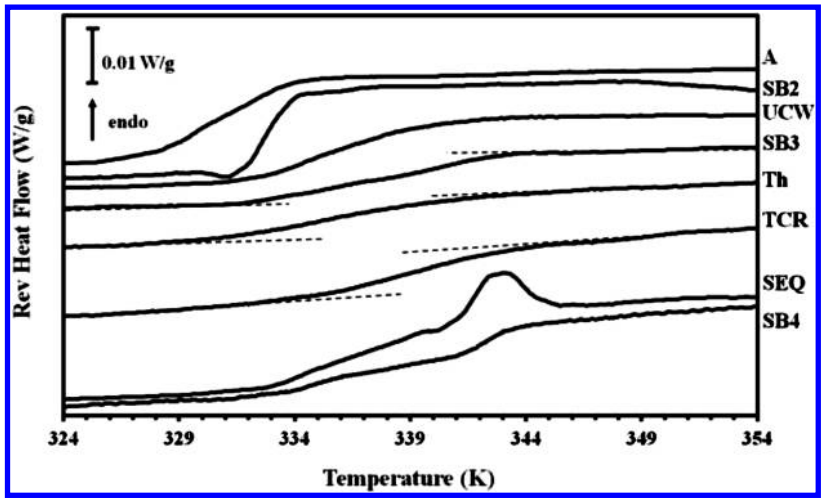

Figure 5. Reversing heat flow versus temperature.

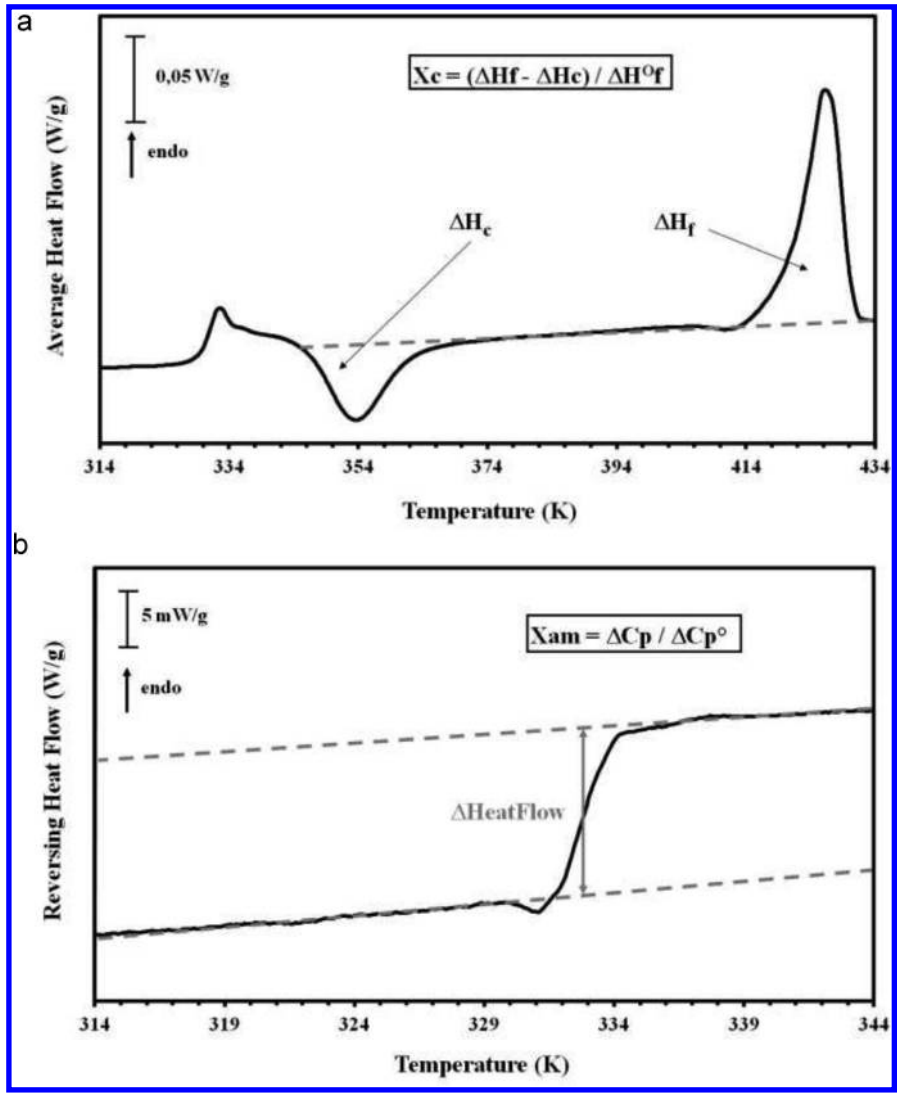

Figure 6. (a) Average heat flow and (b) reversing heat flow versus temperature for the simultaneous biaxial drawn SB2 material. Equation details the calculation of the crystallinity degree X_c and the mobile amorphous phase degree X_{am}.

model is suitable to describe the microstructure of these materials by considering a vitreous phase and a crystalline phase. On the contrary, in the thermally crystallized PLA $X_c + X_{am}$ is lower than 1 and a third fraction is added. This third fraction is called the rigid amorphous fraction (RAF), with X_{ar} being its content. The RAF is defined as a part of the amorphous phase

dx.doi.org/10.1021/jp211670g | J. Phys. Chem. B 2012, 116, 4615–4625

Table 1. Crystallinity Degree (X_c), Mobile Amorphous Phase Degree (X_{am}), Rigid Amorphous Fraction Degree (X_{ar}), Transport Property Parameters in the Different Materials: Permeability Coefficient P, Diffusion Coefficients at the Inflection Time D_I, and at the Time-Lag D_L, Diffusion Coefficients at Nil Concentration D_0, at Equilibrium Concentration D_M, and Plasticization Coefficient γ

	X_c (%) ± 4	X_{am} (%) ± 2	X_{ar} (%) ± 6	P (10^{-12} mol m^{-1} s^{-1} Pa^{-1}) ± 0.07 × 10^{-12}	D_I (10^5 m^2 s^{-1}) ± 0.6 × 10^5	D_L (10^5 m^2 s^{-1}) ± 0.6 × 10^5	D_0 (10^5 m^2 s^{-1}) ± 0.5 × 10^5	D_M (10^5 m^2 s^{-1}) ± 0.7 × 10^5	γ ± 0.04
amorphous film	0	100	0	2.15	21.9	30.3	8.7	175.0	2.91
thermally crystallized film (T_c = 353 K)	31	41	28	2.04	24.3	32.1	14.9	113.0	1.67
UCW drawn material (3 × 1)	28	66	6	2.04	8.3	10.8	4.7	43.3	0.66
SEQ drawn material (3 × 3)	27	70	3	1.97	4.9	5.6	3.8	13.2	0.16
SB drawn material (2 × 2)	13	86	1	1.76	7.4	11.2	2.2	72.3	1.36
SB drawn material (3 × 3)	25	66	9	1.63	2.5	3.0	1.8	9.0	0.15
SB drawn material (4 × 4)	31	62	7	1.63	1.2	1.5	0.7	6.5	0.12
SB drawn (3 × 3) thermofixed material	31	59	10	1.70	4.4	4.9	3.3	13.5	0.21

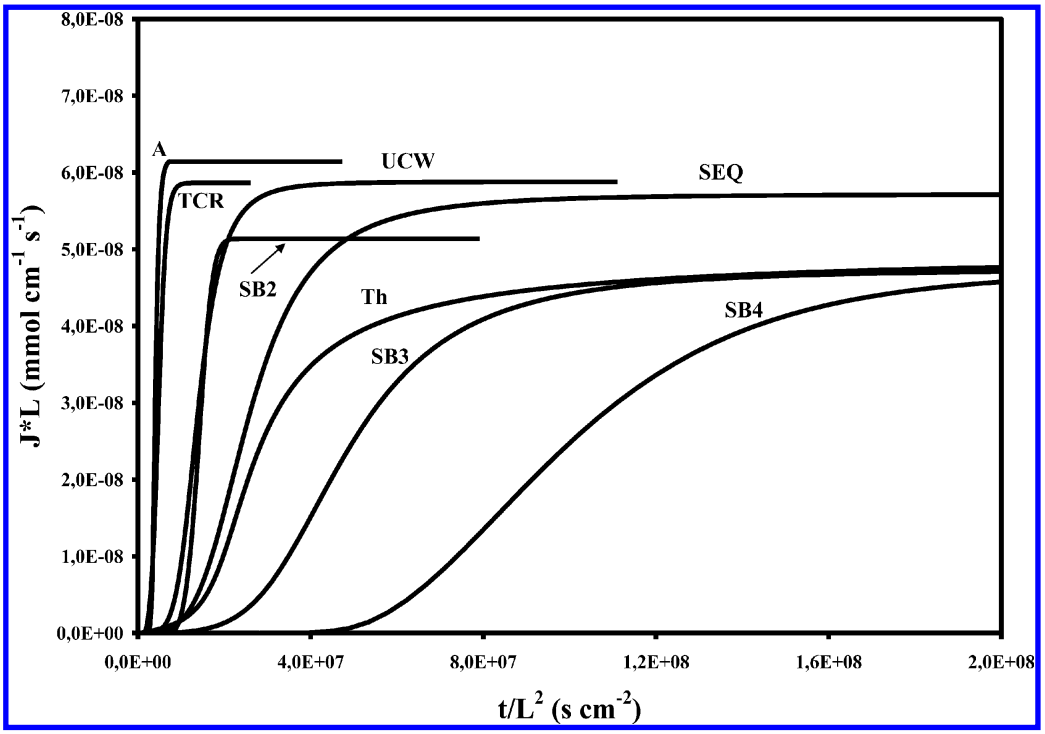

Figure 7. Reduced flow (J,L) versus reduced time (t/L^2) for the different films. A is the amorphous material, TCR is the thermally crystallized material (T_c = 353 K), UCW is the uniaxial constant width drawn material with a draw ratio of 3 × 1, SEQ is the sequential drawn material with a draw ratio of 3 × 3, SB2 is the simultaneous biaxial drawn material with a draw ratio of 2 × 2, SB3 is the simultaneous biaxial drawn material with a draw ratio of 3 × 3, SB4 is the simultaneous biaxial drawn material with a draw ratio of 4 × 4, Th is the thermofixed simultaneous biaxial drawn material with a draw ratio of 3 × 3.

which does not participate to the glass transition,[52,53] and it has already been identified in thermally crystallized PLA.[54−56] In the thermally crystallized PLA the important RAF degree is due to the spherulitic microstructure where crystalline lamellas confine amorphous domains in such a way that the decoupling between crystalline and amorphous phases is incomplete involving a decrease of the amorphous phase chain mobility.[57]

The water permeation results are shown in Figure 7 by representing the flux curves in the reduced scale (J.L as a function of t/L^2). This scale allows the comparison of the permeation flux curves of samples having different thickness. It appears first that the amorphous and the thermally crystallized samples exhibit almost the same behavior. This is in agreement with recent results from Cocca et al.[25] reporting that α crystallization is more efficient to increase water barrier properties than α' crystallization. A decrease of ∼40% of the permeability to water vapor with very small increase of crystal fraction is correlated to the varied ratio of α to α' crystal modification. So, it can be inferred that the differences in molecular packing between α and α' forms influence the permeability coefficient. Cocca et al. speculated that the tighter

dx.doi.org/10.1021/jp211670g | J. Phys. Chem. B 2012, 116, 4615−4625

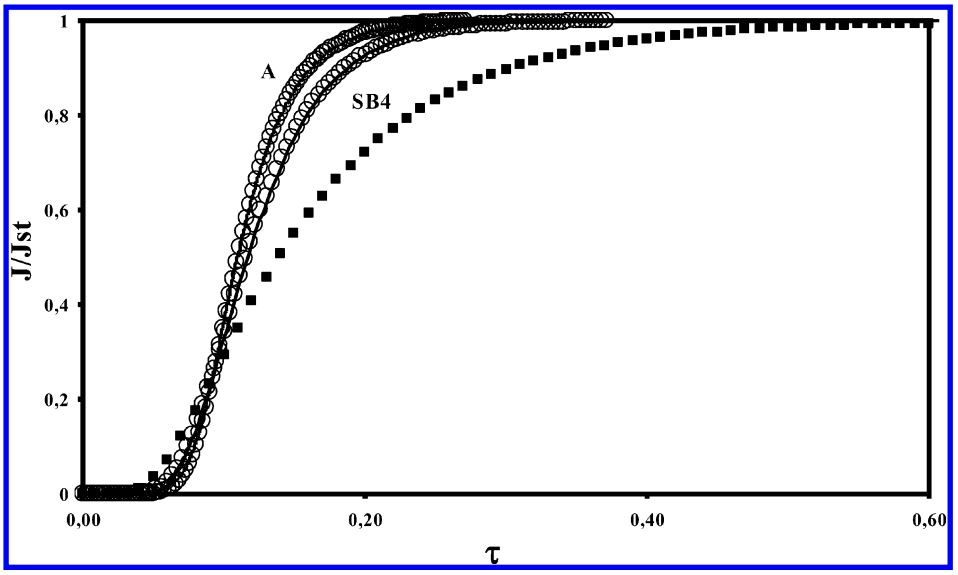

Figure 8. Simulation examples of the permeation kinetics. The black squares correspond to the theoretical curve D = constant. The continuous curves are the experimental curves. The circles correspond to the simulation with $D = D_0 \exp(\gamma C)$. A is the amorphous film, and SB4 is the SB drawn material with a draw ratio of 4 × 4.

molecular packing of PLLA chain segments in α modification, combined with the strong coupling with the amorphous portions of the macromolecules, may reduce diffusion of the adsorbed water vapor through the PLLA films. Regarding the influence of stretching, results show that the delay time is always higher for the drawn material than for both amorphous and thermally crystallized materials independently of the drawing mode used. Moreover, the delay time is found to be higher for a biaxially drawn PLA than for a uniaxially drawn PLA. Also, this parameter increases with increasing the draw ratio. Finally at comparable draw ratios the higher delay time is obtained with the SB drawing mode. Regarding the influence of a thermal post-treatment, it is worth noticing that the thermofixation leads to a decrease of the delay time. It means that water molecules diffuse more easily into the material after this treatment.

The permeability coefficients P are calculated by using eq 3 and from the steady state of the reduced flux (J,L) curves (see Table 1). The uncertainties were fixed by taking the most important difference between two films of the same nature i.e. in our case between two amorphous PLA. This difference was reported on all films. Compared to the amorphous PLA, a slight decrease of the permeability coefficient is observed for the SEQ drawn and the UCW films, whereas a significant decrease is obtained for the SB drawn materials and particularly for the high draw ratios (λ = 3 × 3, λ = 4 × 4). Indeed P decreases from 2.15 ± 0.07 × 10^{-12} for the amorphous film to 1.63 ± 0.07 × 10^{-12} mol m^{-1} s^{-1} Pa^{-1} for a SB drawn film with a draw ratio of 3 × 3 or 4 × 4, i.e., a permeability decrease of 25%. Finally, no significant difference is observed between a thermofixed and a nonthermofixed material. The diffusion coefficients D_I and D_L are calculated for each film by using eqs 4 and 5 and are reported in Table 1. Besides the fact that the obtained values are consistent with the delay times and the permeability coefficients previously calculated (i.e., lower diffusion coefficients for the drawn materials and particularly for SB drawn materials and when the draw ratio is high), it appears that D_L is always higher than D_I.

4. DISCUSSION

Results show that drawing PLA induces a close evolution between its structure and its water barrier properties. The first observable link between permeation and microstructure, i.e., crystalline texture and amorphous phase topology, is the time necessary to observe the water passage through the films. Regarding isotropic materials the delay time does not increase for the thermally crystallized PLA since α' form does not influence the water barrier properties. As explained by Cocca et al.,[25] when PLA crystallizes under the α' crystalline form, the effect of crystallinity on water barrier properties is nil. In opposition the delay time increases slightly when the orthotropic crystalline structure exists but is not optimal i.e. for the UCW and the SB2 samples. For the SB3 and SB4 samples, where a strong crystalline texture is observed, the delay times are the highest. This arises in the fact that the denser planes are lying in the plane of the film due to the strong texturation. Moreover it can be assumed that the preferential crystallite orientation in the film plane for SB3 and SB4 is also accompanied with a preferential orientation of the macromolecules in the same plane, i.e., perpendicular to the water passage. As a consequence the macromolecule orientation also plays a barrier role. This is confirmed regarding the thermofixed sample where both the crystalline and the amorphous phase anisotropies decrease, leading to a decrease of the delay time. Thus, the macromolecule orientation clearly impacts the delay time for water permeation.

The fact that D_L is always higher than D_I is often observed in thermoplastics and is generally related to the polymer plasticization by water molecules. Assuming the latter, a model taking into account a possible variation of D with the concentration C of sorbed molecules can be applied.[58] The diffusion coefficient is usually assumed to increase exponentially with the local permeant concentration in the film during the course of water penetration.[59] This is generally attributed to a free volume increase because of the material plasticization by the permeant[60,61] and this can be modeled by the equation

$$D = D_0 \exp(\gamma C) \quad (6)$$

dx.doi.org/10.1021/jp211670g | J. Phys. Chem. B 2012, 116, 4615−4625

where D_0 is the diffusion coefficient at nil concentration, γ is the plasticization coefficient, and C is the local concentration of sorbed molecules.[37] To determine the two parameters of this diffusion law, a method previously described in ref 36 has been used. The fitting procedure of the experimental transient flux data allows computing the values of D_0 and γ. D_0, the kinetic parameter of the dry polymer, depends on the material microstructure. The plasticization coefficient γ (expressed in cm^3/mol) is correlated to the free volume induced by the presence of diffusing molecules inside the material.[37] Thus the diffusion coefficient varies between D_0 and D_M with D_M defined by

$$D_M = D_0 \exp(\gamma C_{eq}) \quad (7)$$

where C_{eq} is the equilibrium water concentration and D_0 corresponds to the diffusion of the first water molecules in the lack of dependence with the water concentration. In that way, it gives information about the microstructure influence on the water transfer. D_M corresponds to the water mobility in the plasticized material, so that it debriefs about the material plasticization degree. The values of D_0 and D_M are given in Table 1.

The permeation curves are plotted in a dimensionless scale of flux (J/J_{st}) and time ($\tau = D_1 t/L^2$).[62] As an example, the simulations for the two extreme cases, i.e. the amorphous film and the SB4, are plotted in Figure 8. In each case, the experimental curve and the theoretical one calculated for D constant are not superimposed. On the other hand the chosen exponential law of D with C allows a very good fitting of the experimental data.

Results show that drawing has a pronounced impact on an amorphous film involving an important decrease of D_0 and γ. The macromolecule orientation and the creation of oriented crystallites in the drawn materials disturb the diffusion of the first water molecules. So D_0 is very low for the drawn materials as compared to an amorphous one. The most important decrease of D_0 is observed after biaxial drawing, especially for SB drawing. Not only does the orthotropic microstructure disturb the diffusion of the first water molecules but it also has a high preventing effect against plasticization. Moreover, the higher the elongation ratio, the lower γ, even if the drawing mode has a more pronounced effect than the draw ratio on the first molecule diffusion since D_0 is lower for the SB2 than for the SEQ and the UCW. It has been shown previously that plasticization occurs in all materials, but it is clear that some materials are more sensitive to plasticization than others. Thus, the amorphous film exhibits the highest plasticization coefficient ($\gamma = 2.91$). In comparison, γ is really low for the drawn materials, excepted for the SB2 ($\gamma = 1.36$). In the amorphous film case, it is not surprising to observe a significant increase of the water diffusivity during the permeation process, this being due to the high plasticization level. The behavior observed for the SB2 sample is different: the water barrier effect has been limited because the plasticization is higher than for other drawn materials. Concerning the UCW and the biaxially drawn PLA, some differences can be observed: The plasticization coefficient is higher in the UCW drawn material ($\gamma = 0.66$) than in the biaxially drawn materials ($\gamma \leq 0.21$). This is the most significant when the macromolecules are oriented in the film plane and especially for an orthotropic orientation. From D_M and γ values, we deduce that the amorphous phase orientation prevents the amorphous phase plasticization, inducing a huge increase of the diffusion coefficient during the water passage. While D_M/D_0 and γ are respectively equal to 20 and 2.9 for an amorphous sample, $D_M/D_0 = 9$ and $\gamma = 0.66$ for the UCW, and $D_M/D_0 = 5$ and $\gamma = 0.15$ for the SB3. In other words, the water barrier properties are better in biaxially drawn materials (with a draw ratio at least equal to 3×3). An important fact arising from this study is the strong influence of the macromolecular orientation on the PLA water barrier behavior.

The permeation parameters of the wholly amorphous and the thermally crystallized samples are relatively similar showing that the permeability is not directly proportional to the degree of the mobile amorphous phase. As others authors,[25] we put in evidence that barrier properties are weakly dependent on the crystallinity degree in the case of α' spherulitic semicrystalline PLA. One can suppose that in α' semicrystalline PLA the crystalline phase organization is imperfect and an important quantity of RAF exists.[25] The RAF vitrified for some polymers at the crystallization temperature higher than T_g suggesting a smaller density than the MAP density.[63] A recent PALS study on PLA has shown that the crystallization at 100 °C induced a dedensification causing an increase of the free volume fraction.[64] This is an important result because it explains why in our study D_0 is higher in the thermally crystallized PLA than in the amorphous PLA. D_M does not evolve since the presence of crystals reduces plasticization.

Comparison between the two biaxially drawn samples (i.e., SEQ and SB) reveals that the permeability P and the diffusion coefficients D are quite lower for the SB. This result is in accordance with some observations concerning the microstructure of a SEQ drawn material.[65] A process of sequential biaxial drawing is dividing into two steps. First, the material is drawn in the longitudinal direction. At that time, the material microstructure is identical to those of a uniaxially drawn material. Nevertheless, during the second step, the material is drawn in a direction perpendicular to the first one, i.e., the transversal direction. Consequently, as confirmed in Figure 2, the macromolecules are preferentially oriented in the two drawing directions in the film plane. But this second drawing step leads also to a redistribution of the chain orientation from the longitudinal direction to the transversal direction.[44] This ends up in a partial destruction of the crystallites initially oriented in the longitudinal direction, and in the imperfect crystal appearance oriented in the transversal direction.[44,45]

In the same way, the barrier properties are also different between the drawn materials having the same crystallinity degree. Once again, it can be conclude that the crystallinity degree seems to play a minor role on the drawn material barrier properties. The delay time is more important for the biaxially drawn materials than for the UCW drawn materials, and the significant permeability coefficient variation is only obtained for the SB drawn materials having a draw ratio of 3×3. Looking at these results, it appears that the water diffusion is more difficult when the PLA macromolecules are oriented in the film plane, i.e., perpendicularly to the water molecule diffusion. In the case of SB drawing process, the macromolecules are oriented homogeneously in the plane of the film. Thus, the orthotropic structure resulting from SB drawing seems the more efficient to increase the PLA barrier properties as confirmed by the diffusion coefficient values.

DSC curves (Figures 4 and 5) show that the amorphous phase behavior is also influenced by the thermofixation process application. A stabilization of the sample at 120 °C during 5 min after the drawing process implies a decrease of the mobile amorphous phase degree. However the water barrier

dx.doi.org/10.1021/jp211670g | J. Phys. Chem. B 2012, 116, 4615–4625

properties decrease. Compared to a nonthermofixed material, it causes a delay time decrease and an increase of the diffusion and plasticization coefficients. Eventually, the thermofixed material exhibits a higher D_0 coefficient ($D_0 = 3.3 \times 10^9$ cm^2 s^{-1}) compared to the nonthermofixed material ($D_0 = 1.8 \times 10^9$ cm^2 s^{-1}). It has been shown that an annealing above the glass transition can modify the PLA microstructure.[66] Indeed the thermofixation process induces a constraint slackening in the amorphous phase which may be assimilated as an increase of the free volume fraction.

Strategies allowing an increase of water barrier properties are given in the literature: the introduction of 5% montmorillonite (w/w) in PLA generates a decrease of 40% on the water vapor transmission rate.[11] In the same way, the double coating of polyelectrolyte multilayer and Al_2O_3 is found to enhance in 50% the water vapor barrier properties of the PLA film.[67] We show here that beyond chemical modifications, the increase of tortuosity plays also a very high role in the diffusivity decrease, and consequently in the barrier property improvement.

5. CONCLUSION

The drawing process generates a macromolecular reorganization in PLA, modifying the amorphous phase behavior. Because of the tortuous pathway increase in the drawn materials, the water diffusivity is reduced limiting the water molecule access inside the material: the plasticization becomes less efficient and the water barrier properties are improved. We show here that the crystallinity degree is not sufficient to predict the water permeation behavior of a material since the water barrier properties are more dependent on amorphous phase conformation. The water molecule diffusion is a complex mechanism and more parameters such as the diffusion direction and the crystallite orientation in the film plane have to be considered. The study of the material microstructure shows that the orthotropic structure, issued from SB drawing (the macromolecules are oriented homogeneously in the film plane) leads to the most disturbing effect for the water passage. The process is limited by the PLA brittle character when the draw ratio and the crystallinity degree are too high. As a consequence, it can be assumed that the limit decrease of permeability has been approached in this work. Nevertheless, the drawn PLA remains 20 times more permeable than Poly(ethylene terephthalate). This decrease is considered as insufficient and other strategies have to be developed. We must keep in mind that the water resistance remains one of the main criteria to develop this kind of biodegradable polymer as new packaging material. From that, the knowledge of the relation between the PLA microstructure and the water barrier properties still plays an important part in the improvement of PLA behavior against molecule diffusion.

AUTHOR INFORMATION

Corresponding Author

*(G.S.) Tel: 00333 20 43 49 13. Fax: 00333 20 43 65 91. E-mail: gregory.stoclet@univ-lille1.fr. (E.D.) Tel: 00332 32 95 50 80. Fax: 00332 32 95 50 82. E-mail: eric.dargent@univ-rouen.fr.

Notes

The authors declare no competing financial interest.

REFERENCES

(1) Auras, R.; Harte, B.; Selke, S. *Macromol. Biosci.* **2004**, *4*, 835−864.
(2) Drumright, R. E.; Gruber, P. R.; Henton, D. E. *Adv. Mater.* **2000**, *12*, 1841−1846.
(3) Garlotta, D. *J. Polym. Environ.* **2001**, *9*, 63−84.
(4) Rhim, J. W.; Hong, S. I.; Ha, C. S. *LWT--Food Sci. Technol.* **2009**, *42*, 612−617.
(5) Chaiwong, C.; Rachtanapun, P.; Wongchaiya, P.; Auras, R.; Boonyawan, D. *Surf. Coat. Technol.* **2010**, *204*, 2933−2939.
(6) Auras, R.; Harte, B.; Selke, S.; Hernandez, R. *J. Plast. Film Sheeting* **2003**, *19*, 123−135.
(7) Auras, R.; Singh, S. P.; Singh, J. *J. Packag. Technol. Sci.* **2005**, *18*, 207−216.
(8) Holm, V. K.; Ndoni, S.; Risbo, J. *J. Food Sci.* **2006**, *71*, E40−E44.
(9) Incarnato, L.; Di Maio, L.; Garofalo, E.; Scarfato, P. *AIP Conf. Proc.* **2010**, *1255*, 364−366.
(10) Maiti, P.; Yamada, K.; Okamoto, M.; Ueda, K.; Okamoto, K. *Chem. Mater.* **2002**, *14*, 4654−4661.
(11) Zenkiewicz, M.; Richert, J.; Rozanski, A. *Polym. Test.* **2010**, *29*, 251−257.
(12) Sanchez-Garcia, M. D.; Gimenez, E.; Lagaron, J. M. *Carbohydr. Polym.* **2008**, *71*, 235−244.
(13) Fortunati, E.; Armentano, I.; Iannoni, A.; Kenny, J. M. *Polym. Degrad. Stab.* **2010**, *95*, 2200−2206.
(14) Gorrasi, G.; Vittoria, V.; Murariu, M.; Da Silva Ferreira, A.; Alexandre, M.; Dubois, P. *Biomacromolecules* **2008**, *9*, 984−990.
(15) Suyatma, N. E.; Copinet, A.; Tighzert, L.; Coma, V. *J. Polym. Environ.* **2004**, *12*, 1−6.
(16) Cho, S. W.; Gallstedt, M.; Hedenqvist, M. S. *J. Agric. Food Chem.* **2010**, *58*, 7344−7350.
(17) Kanehashi, S.; Kusakabe, A.; Sato, S.; Nagai, K. *J. Membr. Sci.* **2010**, *365*, 40−51.
(18) Komatsuka, T.; Kusakabe, A.; Nagai, K. *Desalination* **2008**, *234*, 212−220.
(19) Colomines, G.; Domenek, S.; Ducruet, V.; Guinault, A. *Int. J. Mater. Form.* **2008**, *1*, 607−610.
(20) Colomines, G.; Ducruet, V.; Courgneau, C.; Guinault, A.; Domenek, S. *Polym. Int.* **2010**, *59*, 818−826.
(21) Tsuji, H.; Okino, R.; Daimon, H.; Fujie, K. *J. Appl. Polym. Sci.* **2006**, *99*, 2245−2252.
(22) De Santis, P.; Kovacs, J. *Biopolymers* **1968**, *6*, 299−306.
(23) Sasaki, S.; Asakura, T. *Macromolecules* **2003**, *36*, 8385−8390.
(24) Zhang, J.; Tashiro, K.; Tsuji, H.; Domb, A. J. *Macromolecules* **2008**, *41*, 1352−1357.
(25) Cocca, M.; Di Lorenzo, M. L.; Malinconico, M.; Frezza, V. *Eur. Polym. J.* **2011**, *47*, 1073−1080.
(26) Masirek, R.; Piorkowska, E.; Galeski, A.; Mucha, M. *J. Appl. Polym. Sci.* **2007**, *105*, 282−290.
(27) Liu, R. Y. F.; Schiraldi, D. A.; Hiltner, A.; Baer, E. *J. Polym. Sci. Part B: Pol. Phys.* **2002**, *40*, 862−877.
(28) Orchard, G. A. J.; Spiby, P.; Ward, I. M. *J. Polym. Sci., Part B: Polym. Phys.* **1990**, *28*, 603−621.
(29) Mulligan, J.; Cakmak, M. *Macromolecules* **2005**, *38*, 2333−2344.
(30) Stoclet, G.; Seguela, R.; Lefebvre, J. M.; Elkoun, S.; Vanmansart, C. *Macromolecules* **2010**, *43*, 1488−1498.
(31) Stoclet, G.; Seguela, R.; Lefebvre, J. M.; Rochas, C. *Macromolecules* **2010**, *43*, 7228−7237.
(32) Stoclet, G.; Seguela, R.; Lefebvre, J. M.; Li, S.; Vert, M. *Macromolecules* **2011**, *44*, 4961−4969.
(33) Sallem-Idrissi, N.; Miri, V.; Elkoun, S.; Krawczak, P.; Lacrampe, M. F.; Lefebvre, J. M.; Seguela, R. *Polymer* **2009**, *50*, 5812−5823.
(34) Crank, J.; Park, G. S. *Methods of measurement*. In Crank, J., Park, G. S., Eds.; *Diffusion in polymers*; Academic Press: London, 1968; pp 1−40.
(35) Carslaw, H. S.; Jaeger, J. C. *Conduction of heat in solid*, 2nd ed.; Oxford University Press: London, 1959; Chapters 3 and 12.
(36) Marais, S.; Métayer, M.; Labbé, M. *J. Appl. Polym. Sci.* **1999**, *74*, 3380−3395.
(37) Marais, S.; Nguyen, Q. T.; Devallencourt, C.; Métayer, M.; Nguyen, T. U.; Schaetzel, P. *J. Polym. Sci., Part B: Polym. Phys.* **2000**, *38*, 1998−2008.

(38) Archer, D. G.; Rudtsch, S. *J. Chem. Eng. Data* **2003**, *48*, 1157−1163.
(39) Lacey, A. A.; Price, D. M.; Reading, M. Theory and Practice of Modulated Temperature Differential Scanning Calorimetry. In Reading, M., Hourston, D. J., Eds.; *Modulated temperature differential scanning calorimetry: theoretical and practical applications in polymer characterisation*; Springer: Dordrecht, The Netherlands 2006; pp 1−81.
(40) Fischer, E. W.; Sterzel, H. J.; Wegner, G. *Colloid Polym. Sci.* **1973**, *251*, 980−990.
(41) Reading, M.; Elliot, D.; Hill, V. L. *Proc. 21st North Am. Therm. Anal. Soc. Conf.* **1992**, *20*, 145−150.
(42) Reading, M.; Hahn, B. K.; Crowe, B. S. *Method and Apparatus for Modulated Differential Analysis*; U.S. Patent 5,224,775, 1993.
(43) Pelletier, I.; Laurin, I.; Buffeteau, T.; Pezolet, M. *J. Phys. Chem. B* **2004**, *108*, 7162−7169.
(44) Ou, X.; Cakmak, M. *Polymer* **2008**, *49*, 5344−5352.
(45) Ou, X.; Cakmak, M. *Polymer* **2010**, *51*, 783−792.
(46) Yasuniwa, M.; Sakamo, K.; Ono, Y.; Kawahara, W. *Polymer* **2008**, *49*, 1943−1951.
(47) Kulinski, Z.; Piorkowska, E. *Polymer* **2005**, *46*, 10290−10300.
(48) Janssens, S.; Denivelle, S.; Rombaut, P.; Van den Mooter, G. *Eur. J. Pharm. Sci.* **2008**, *35*, 203−210.
(49) Delpouve, N.; Lixon, C.; Saiter, A.; Dargent, E.; Grenet, J. *J. Therm. Anal. Calorim.* **2009**, *97*, 541−546.
(50) Adams, G. W.; Farris, R. J. *Polymer* **1989**, *30*, 1829−1835.
(51) Martin, B.; Wondraczek, L.; Deubener, J.; Yue, Y. *Appl. Phys. Lett.* **2005**, *86*, 1219171−1219173.
(52) Menczel, J.; Wunderlich, B. *J. Polym. Sci. Part C: Polym. Lett.* **1981**, *1*, 261−264.
(53) Suzuki, H.; Grebowicz, J.; Wunderlich, B. *Br. Polym. J.* **1985**, *17*, 1−3.
(54) Chen, H.; Pyda, M.; Cebe, P. *Thermochim. Acta* **2009**, *492*, 61−66.
(55) Saiter, A.; Delpouve, N.; Dargent, E.; Saiter, J. M. *Eur. Polym. J.* **2007**, *43*, 4675−4682.
(56) Delpouve, N.; Saiter, A.; Mano, J. F.; Dargent, E. *Polymer* **2008**, *49*, 3130−3135.
(57) Arnoult, M.; Dargent, E.; Mano, J. F. *Polymer* **2007**, *48*, 1012−1019.
(58) Lixon Buquet, C.; Ben Doudou, B.; Chappey, C.; Dargent, E.; Marais, S. *J. Phys. Chem. B* **2009**, *113*, 3445−3452.
(59) Long, R. B. *Ind. Eng. Chem. Fundam.* **1965**, *4*, 445−451.
(60) Prager, S.; Long, F. A. *J. Am. Chem. Soc.* **1951**, *73*, 4072−4075.
(61) Stern, S. A.; Trohalaki, S. *barrier polymer and barrier structures; ACS Symposium Series*; American Chemical Society: Washington, DC, 1990; Chapter 2, pp 22−59.
(62) Follain, N.; Valleton, J. M.; Lebrun, L.; Alexandre, B.; Schaetzel, P.; Metayer, M.; Marais, S. *J. Membr. Sci.* **2010**, *349*, 195−207.
(63) Ma, Q.; Georgiev, G.; Cebe, P. *Polymer* **2011**, *52*, 4562−4570.
(64) del Rio, J.; Etxebarria, A.; Lopez-Rodriguez, N.; Lizundia, E.; Sarasua, J. R. *Macromolecules* **2010**, *43*, 4698−4707.
(65) Gohil, R. M.; Salem, D. R. *J. Appl. Polym. Sci.* **1993**, *47*, 1989−1998.
(66) Takahashi, K.; Sawai, D.; Yokoyama, T.; Kanamoto, T.; Hyon, S. H. *Polymer* **2004**, *45*, 4969−4976.
(67) Hirvikorpi, T.; Vaha-Nissi, M.; Harlin, A.; Salomaki, M.; Areva, S.; Korhonen, J. T.; Karppinen, M. *Appl. Surf. Sci.* **2011**, *257*, 9451−9454.